Effect of perovskite as an HTL on the enhancement of efficiency of CIGSSe photovoltaics device

Rajeev Ranjan Kumar

Associate Professor
Department of Electronics and Communication Engineering
Dr C. V. Raman Unniversity
Bhagwanpur, Vaishali, Bihar.

***Abstract*- In this paper, the performance of the basic (ZnMgO: Al/ZnMgO/CIGSSe) photovoltaic device has been improved by using the novel perovskite as a hole transport layer (HTL) material. At first, the CdS-free basic experimental photovoltaic device with an efficiency of 20% was simulated, and the photovoltaic results were confirmed by entering the experimental optoelectronics data into the AFORS-HET simulation tool. Further, they optimised the thickness and doping density of the basic photovoltaic device's Front , buffer, and absorber layers. After optimization, efficiency (η), V_{OC}, *FF and* J_{SC} have been enhanced, but external quantum efficiency (EQE) is still lesser than basic photovoltaic devices due to the absence of HTL material. Furthermore, a new structure is proposed using perovskite as an HTL material and is added between the CIGSSe/Mo back ohmic metal layers in the optimised photovoltaic device. Therefore, the proposed photovoltaic device absorbs the bulk of blue sunlight, instantly reducing the recombination losses and enhancing the efficiency (27.96%) and EQE.**

Keyword: **Thin-film solar cells, perovskite, External quantum efficiency, hole transport layer, Mg-doped ZnO.**

1. Introduction

Numerous studies look into thin film materials for making affordable, highly efficient solar cells. Due to their low manufacturing costs, high conversion efficiency of 23.35% [1, 2], and stability, chalcopyrite $Cu(In_{1-x}Ga_x)SSe_2$ (Copper Indium Gallium Sulphur Selenide) *p*-type semiconductor materials have recently become more well-liked. Strong *p*-type conductivity, direct adjustable bandgap energy in the range of 1.11-1.69 eV to take advantage of the maximum solar irradiation, and a greatest $3\text{-}6\times10^5$ cm^{-1} absorption coefficient of in the visible light section of the solar spectrum are just a few of the remarkable properties of the compound semiconductor CIGSSe [3–7]. Along with the CIGSSe's absorbing qualities, an *n*-type material is also necessary for a suitable P-N junction. One of the typical materials that has demonstrated a high capacity with CIGSSe because to its transparency is zinc oxide doped with magnesium (ZnMgO). As solar light passes through it, it produces a photovoltaic effect. The direct bandgap of ZnMgO in the visible range is 3.43 eV as well. The ZnMgO/CIGSSe heterojunction cell's front contact requires the transparent conducting oxide (TCO) layer as well. This layer permits photons to enter the cell, and the active interface, which includes zinc oxide doped with aluminium and boron, is thought of as one of the electrodes for gathering current [8]. By minimising the impact of non-uniformity, adding a high transparent-resistive (HTR) film between the TCO and the buffer layer using ZnMgO may increase efficiency. One of the materials utilised as an HTR layer is Magnesium-doped zinc aluminium oxide (ZnMgO:Al).

In the past, a lot of study was done on the back surface field (BSF) layer and how it affected device performance in the 1980s [9-18]. More carriers are attracted to the CIGSSe/BSF heterojunction by using large bandgap materials as barriers, which also helps reduce carrier losses at the back contact. Additionally, by lowering carrier recombination at the rear contact, it improves cell efficiency. Studies in the similar situation have exposed that the use of HTL serves the same purpose as the BSF layer in improving the operation of the photovoltaic device. A perovskite with p-type conductivity and a broad bandgap of 1.0 to 1.7 eV is an appealing option for use as an HTL layer in the CIGSSe solar system [19]. Perovskite has been described as a non-toxic organic substance with high carrier mobility (66 $cm^2/V/s$) [20], long electron-hole diffusion length [21–22], and a great absorption coefficient (1.5×10^4 cm^{-1}] in the visible range. All these perovskite material properties may help enhance the efficiency of the CIGSSe photovoltaic device.

The current study proposes various topologies for CIGS thin film photovoltaic devices. The one-dimensional AFORS-HET simulator is used to numerically analyse the performance of the proposed ZnMgO: Al/ZnMgO/CIGSSe/perovskite thin-film photovoltaic device. Additionally, we show how the device performance is impacted by introducing a perovskite layer as a HTL between the Mo metal contact and CIGSSe layer. In both basic and novel ultra-thin CIGSe photovoltaic devices, the E_g (band of energy) of the perovskite layer as well as the thickness and doping density of the front, buffer, and absorber layers are also explored.

2. Modelling structure and mathematical parameters

In this study, the electrical and optical results of the basic photovoltaic device are produced and validated using the AFORS-HET tool by entering the values of the optical and electrical parameters (provided in Table 1) into the simulation tool. To ascertain the internal electrical properties of the CIGSSe photovoltaic device, the one-dimensional AFORS-HET tool solves the Poisson's equation as well as the electron and hole continuity equations. The Shockley-Read-Hall (SRH) model for bulk defects and an extension of the SRH model for interface defects are used to compute recombination currents. The device's design, the band energy graph, the *J-V* plot, and the EQE versus wavelength curve are shown in Fig. 1(a)–(d). The basic photovoltaic devices' experimental and simulated results are compared in Table 2.

Further, optimising the basic photovoltaic device's Front , buffer, and absorber layer parameters enhanced the efficiency. Still, the EQE kept no changes due to the deficiency of an HTL material. The device structure and band energy illustration of the optimised photovoltaic device are shown in Fig. 2 (a) and 3(a). Further, resolving the above issues by adding the perovskite as an HTL material between the CIGSSe absorber and the molybdenum (Mo) metal contact layer to the proposed new photovoltaic device structure. The performance of the cells is determined by the surface of the CIGSSe films of the proposed device, which shifts the electrical junction away from high recombination at the buffer/absorber interface. The antireflective layering effect of MgF_2 increases photon absorption. There is a discussion of the additional layers in our cell in [13–17]. The device structure and band energy illustration of the proposed photovoltaic device are exposed in Fig. 2 (b) and 3(b).

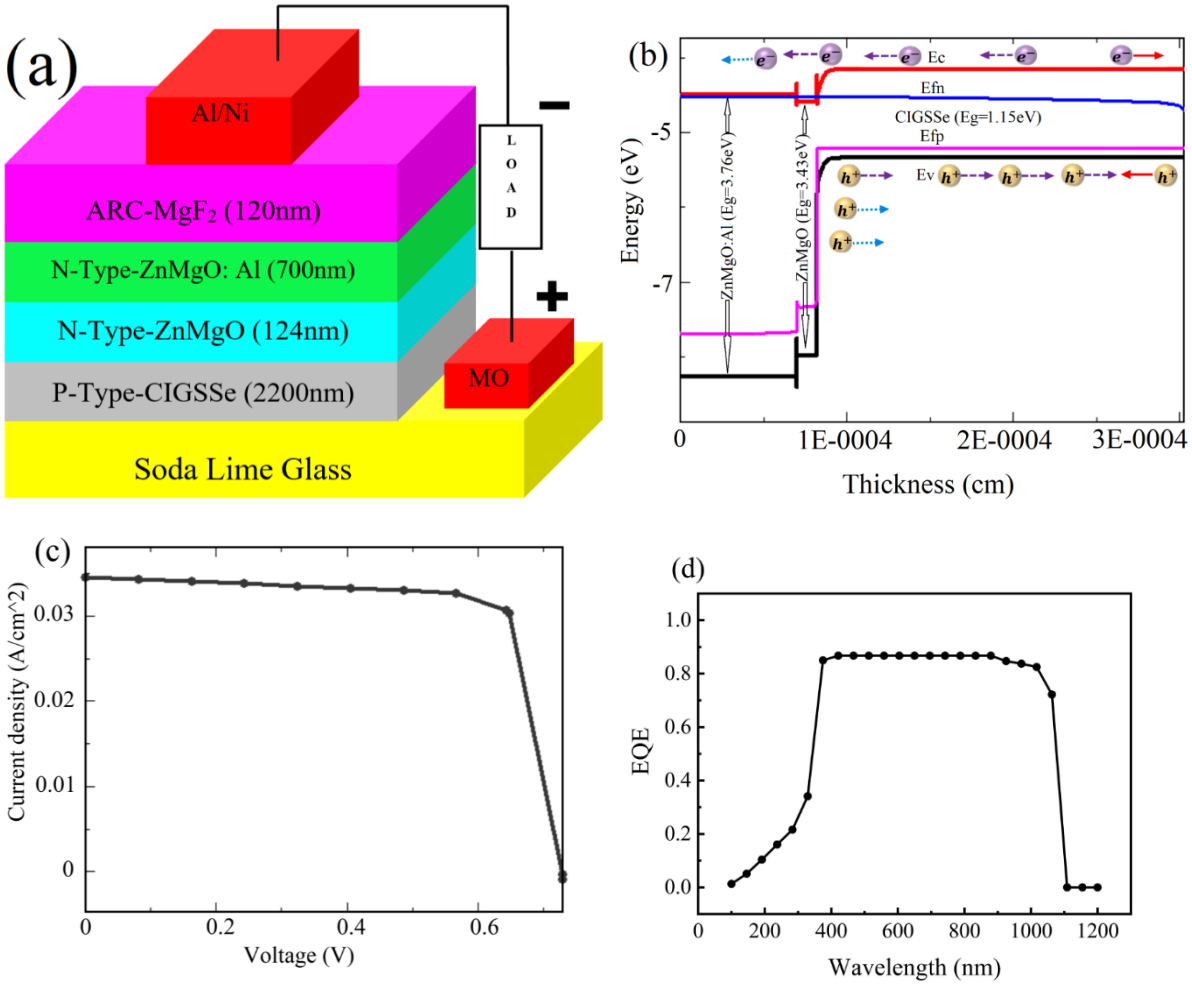

Fig. 1. (a) Arrangement of basic photovoltaic device, (b) band energy sketch, (c) *J-V* plot, and (d) EQE versus wavelength curve of the CIGSSe photovoltaic device [23]

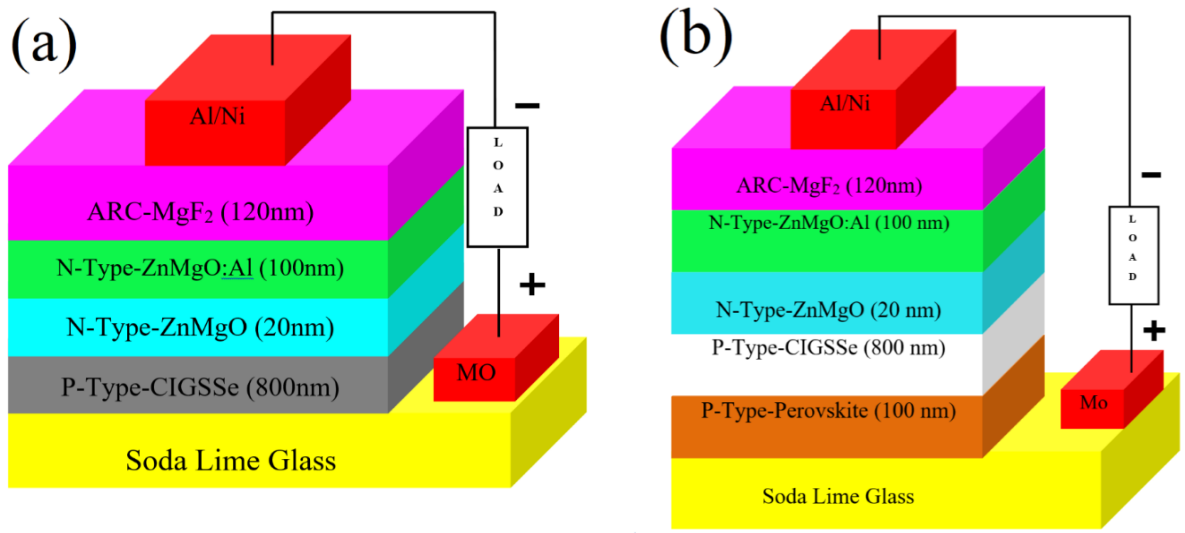

Fig. 2. (a) Optimised photovoltaics device structure and (b) proposed photovoltaics device structure of the CIGSSe solar cell

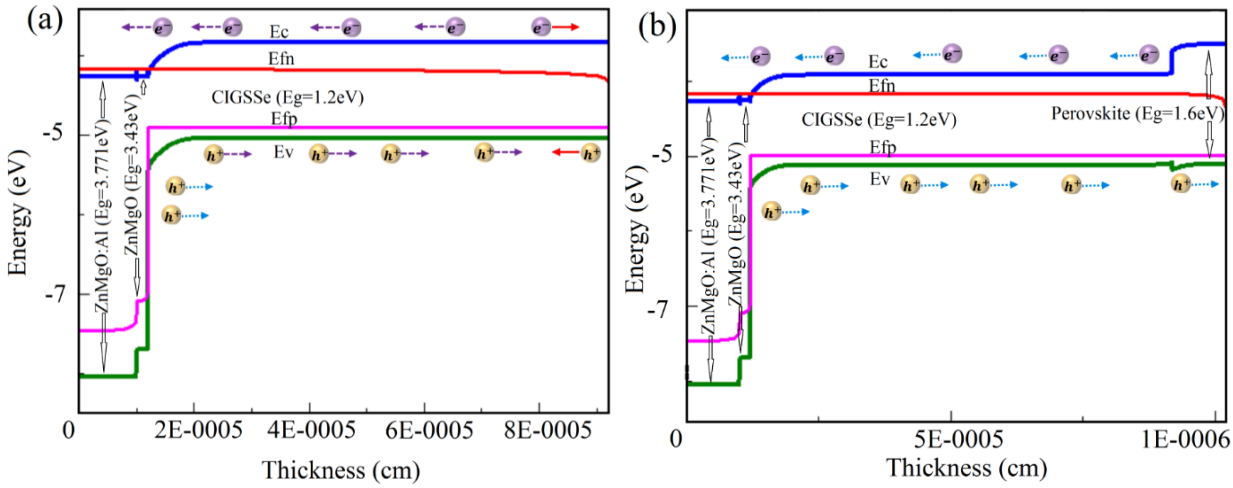

Fig. 3. (a) Band energy diagram of the (a) Optimised photovoltaics device and (b) proposed photovoltaics device.

Table 1: Opto-electronic parameters utilised in the optimised and proposed CIGSSe photovoltaic devices

Electrical Parameters	*n*- (Al-ZnMgO)	*n*-(ZnMgO)	*p*- (CIGSSe)	*p- Perovskite*
Thickness (nm)	100	20	800	100
Energy bandgap E_g (eV)	3.771	3.43	1.2	1.2 to 1.8 (1.6 Highest)
Electron affinity χ (eV)	4.269	4.4	4.26	4.2
Relative permittivity ε_r	10.5	8	13.6	10 [37]
Conduction band effective density of states N_C (cm^{-3})	2.2×10^{18}	3×10^{18}	3.2×10^{18}	3.64×10^{18} [38]
Valance band effective density of states N_V (cm^{-3})	1.8×10^{19}	2×10^{19}	1.5×10^{19}	1.36×10^{19} [38]
Electron mobility μ_e ($cm^2V^{-1}s^{-1}$)	100	50	100	3 [39]
Hole mobility μ_h ($cm^2V^{-1}s^{-1}$)	10	10	25	2 [40]
Donor doping density N_d (cm^{-3})	1×10^{16} to 1×10^{21}	1×10^{16} to 1×10^{21}	0	0
Acceptor doping density N_a (cm^{-3})	0	0	1×10^{15} to 5×10^{17}	1×10^{17}
Electron thermal velocity V_e (cm^2s^{-1})	1×10^{7}	1×10^{7}	3.6×10^{6}	1×10^{7}
Hole thermal velocity V_h (cm^2s^{-1})	1×10^{7}	1×10^{7}	1×10^{7}	1×10^{7}

Auger coefficient of electron R_{ae} (cm^6s^{-1})	2.2×10^{-34}	1.5×10^{-32} [26]	1×10^{-28} [33]	6×10^{-29} [41]
Auger coefficient of hole R_{ah} (cm^6s^{-1})	1.1×10^{-34}	1.2×10^{-32}[26]	1×10^{-28} [33]	1×10^{-29} [41]
Band to band recombination coefficient R_{bb} (cm^3s^{-1})	1.5×10^{-11}	2×10^{-11} [27]	8×10^{-11} [33]	7×10^{-11} [42]
Absorption coefficient α (cm^{-1})	1.2×10^5 [23]	2.2×10^5 [28]	1.45×10^5 [33]	7×10^4 [39]
Resistivity ρ (Ω cm)	1.3×10^{-3} [24]	2×10^{-4} [29]	3×10^4 [34]	1.144×10^3 [39]
R_{Sheet} (Ω/sq.)	18.7 [23]	28.9×10^3 [30]	1×10^2 [35]	1.47×10^9
Intrinsic carrier concentration ηi (cm^{-3})	1×10^{21} [25]	0.246×10^{19} [30]	1×10^{20} [35]	2×10^{15} [39]
Total trap charge density of conduction/valance band tail N_{ttr} (cm^{-3})	1×10^{16}	1×10^{16} [31]	1×10^{14}	1×10^{14} [43]
Electron capture cross section CBT/VBT σ_{te} (cm^2)	3×10^{-14}	5×10^{-13} [31]	1×10^{-14}	1×10^{-17} [43]
Hole capture cross section CBT/VBT σ_{th} (cm^2)	3×10^{-15}	1×10^{-15} [31]	1×10^{-15}	1×10^{-15} [43]
E_urbach (eV)	0.18 [24]	0.531 [32]	0.04 [36]	0.016 [43]

Table 2: Simulation and experimental output results of the three basic CIGSSe TFSCs.

Structure of photovoltaic device	Type of structure	V_{OC} (mV)	J_{SC} (mA/cm^2)	*FF* (%)	η (%)
[(Al/Ni)/MgF_2/ZnMgO:Al/ZnMgO/CIGSSe/Mo] [32]	Experimental	695.00	39.30	73.16	20.00
	Simulation	695.40	39.37	73.41	20.10

3. Results and discussion

4.1. Effects of bandgap energy on the performance CIGSSe/Perovskite proposed TFSC

The basic photovoltaic device lacks the energy required to lessen the photogenerated minority carrier recombination losses seen in the *p*-CIGSSe semiconductor layer without the HTL layer. Furthermore, a proposed inorganic/organic photovoltaic device is created by adding *p*-type perovskite as an HTL between the CIGSSe absorber and Mo back metal contact layer. The inorganic/organic photovoltaic device being presented has enough energy to increase the η (%) and EQE of the structures by decreasing the losses of recombination caused by the carriers minority.

The effect of the perovskite's bandgap energy and electron affinity as an HTL on the performance of the photovoltaic parameters of the proposed photovoltaic device is shown in Table 3. The efficiency (η), V_{OC}, *FF and* J_{SC} constantly rise up to 1.6 eV energy bandgap as the affinity of electron of the CIGSSe layer and the perovskite as an HTL rises. The band energy is directly related to the $V_{OC}=Eg/q$. Additionally, as the height of the barrier rises above the perovskite layer's 1.6 eV band energy, fewer holes are transported towards the back metal contact region and more photogenerated carriers are generated in the *p*-CIGSSe layer. The performance parameters of the proposed photovoltaic device slightly decline while above E_g>16 eV.

Table 3: Fluctuations in the electron affinity and E_g of the perovskite HTL layer cause a deviation in performance metrics.

E_g of perovskite (eV)	χ of perovskite (eV)	V_{OC} (mV)	J_{SC} (mA/cm^2)	*FF* (%)	η (%)
1.2	4.28	775.3	41.28	80.63	25.80
1.3	4.18	806.3	41.59	80.97	27.16
1.4	4.08	808.3	41.60	81.37	27.36
1.5	3.98	810.3	41.61	81.67	27.53
1.6	3.88	815.3	41.67	82.31	27.96
1.7	3.78	808.3	41.63	82.13	27.63
1.8	3.68	807.3	41.59	82.10	27.56

4.2. Impact of thickness and donor doping density of the Al doped ZnMgO front layer

Now, we look into how the front layer's thickness influences the performance of the optimized and CIGSSe/Perovskite based proposed solar cell efficiency. The Al doped ZnMgO front layer thickness for 100 nm and donor carrier density of 10^{20} cm^{-3} are shown to be effective in Fig. 4(a). This variation demonstrates that as ZnMgO: Al thickness rises, cell efficiency falls monotonically. The highest possible level of electrical efficiency might be attained with a ZnMgO: Al

layer that is 100 nm thick. The ZnMgO: Al front layer is where photons first come into contact with the solar cell. As a result, the thickness of the top layer affects how electron-hole pairs occur. A thickness of 100 nm corresponds to the greatest degree of efficiency. This is comparable to earlier discoveries reported in references [44, 45]—Fig. 4(b). As seen in this figure, the efficiency increases with donor carrier density of the front layer ZnMgO: Al between 10^{17} and 10^{21} cm^{-3} and then stays constant at 10^{21} cm^{-3}. It yields a value of 27.96% at 10^{20} cm^{-3} donor carrier density. The rationale for this is that a boost in doping may improve the collection of photogenerated carriers, increasing conversion output. We cap the base's optimised doping level at 10^{20} cm^{-3}. This is consistent with earlier discoveries reported in references [44, 45].

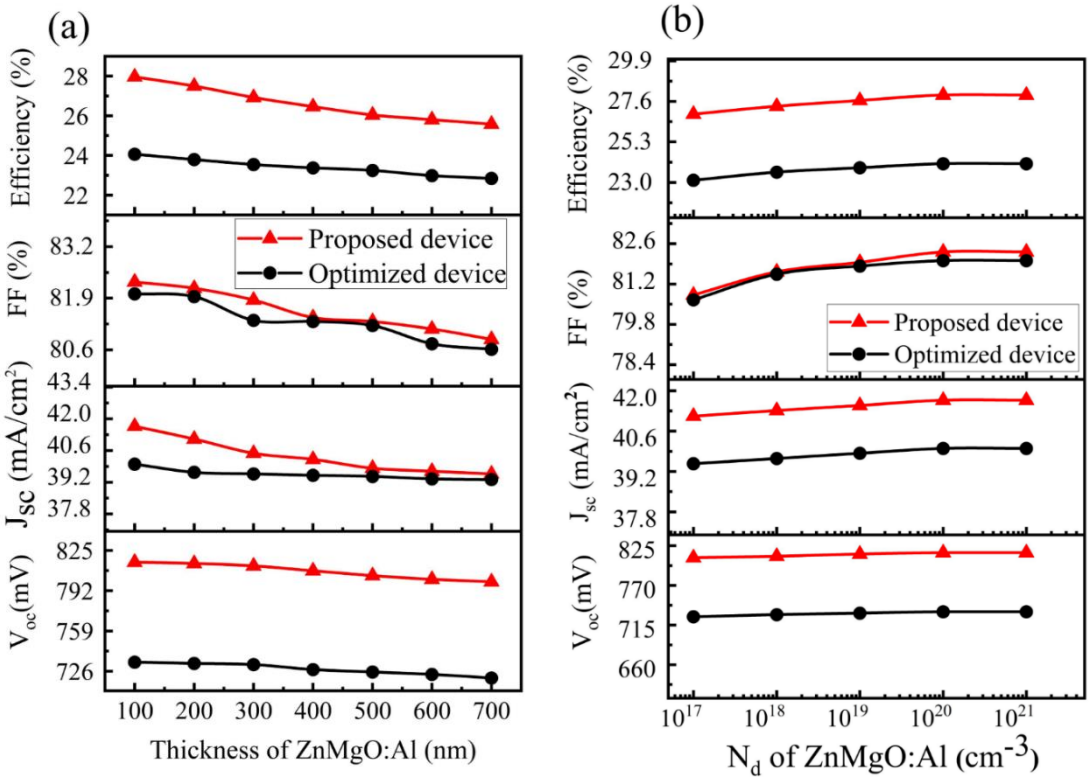

Fig. 4. Difference of η (%), V_{OC}, J_{SC}, and *FF* by the modification of (a) thickness and (b) N_d density of the ZnMgO: Al TCO layer.

4.3. Impact of donor doping density and thickness of ZnMgO buffer layer

As exposed in Figs. 5(a) and (b), the effect of the buffer ZnMgO layer on the cell performance of the optimized and proposed photovoltaic device was investigated (b). The ZnMgO buffer layer's donor carrier density and thickness were adjusted from 10^{17} to 10^{21} cm^{-3} and 10 to 50 nm, respectively. The figures show that the V_{OC}, J_{SC}, *FF*, and efficiency decrease as ZnMgO thickness increases but increase as ZnMgO carrier density increases. The increase in V_{OC}, J_{SC}, *FF*, and efficiency with increasing ZnMgO carrier density of > 10^{20} cm^{-3} demonstrates that recombination of the minority charge carrier reduces with increasing ZnMgO donor carrier density. The rise in fill factor may be accredited to a drop in R_s (series resistance) as donor ZnMgO density increased. This was reflected in the η (%), reaching a maximum efficiency of 27.96 % at ZnMgO carrier density and thickness of 10^{20} cm^{-3} and 20 nm, respectively.

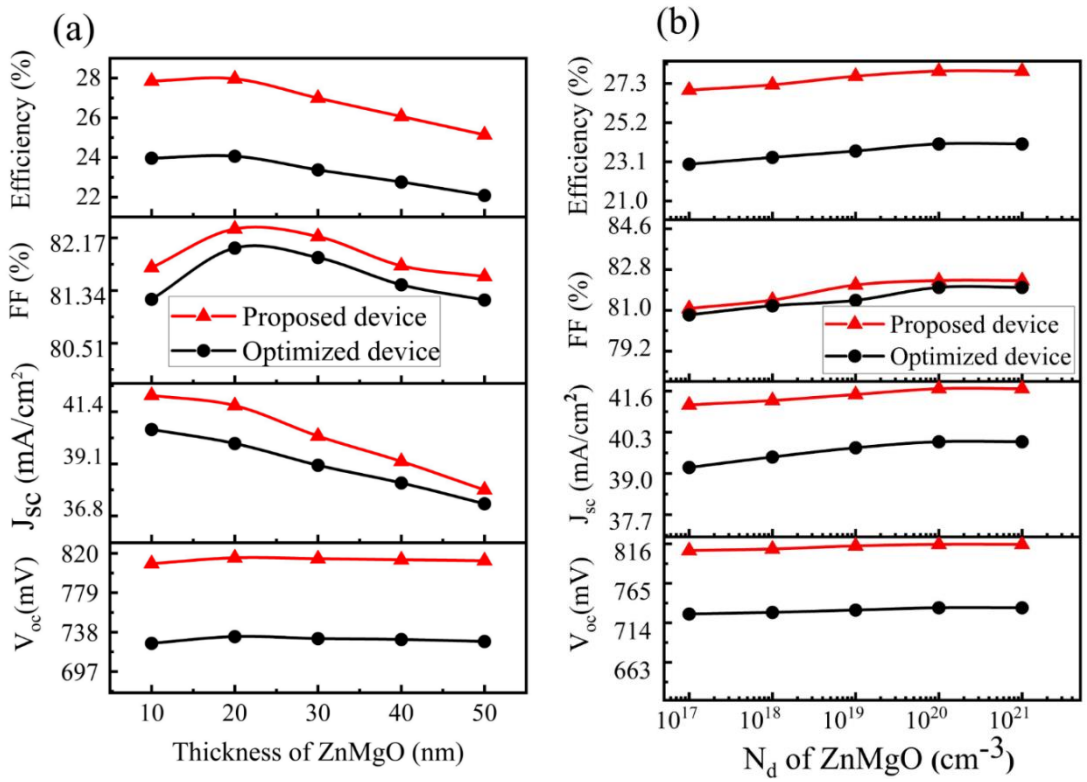

Fig. 5. Variation of V_{OC}, J_{SC}, *FF* and efficiency by the dissimilarity of (a) thickness and (b) donor doping density of the buffer ZnMgO layer.

4.4. Effect of thickness and N_a doping density of the CIGSSe absorber layer

Fig. 6 (a) shows the impact of the optimised and proposed device's CIGSSe thickness on solar efficiency with a fixed carrier density of 1×10^{17} cm^{-3}. We see that the V_{OC}, J_{SC}, *FF*, and efficiency increase monotonically and linearly as CIGSSe thickness increases. More carriers are created when CIGSSe thickness increases. At the time of maximum power, higher current results from more carriers. Furthermore, according to Fig. 6(a), the absorber layer should be as thick as 800 nm, at which time the efficiency of the proposed device will be at its highest or 27.96 %.

Figure 6(b) displays the efficiency variation of the optimized and proposed photovoltaic systems with an 800 nm thickness of CIGSSe films as a function of the acceptor carrier density. The V_{OC}, *FF*, and efficiency quickly improve for the optimised device from 18.44 % to 24.06 % and for the proposed device from 23.25 % to 27.96 % when the acceptor carrier density of the CIGSSe absorber layer is increased from 1×10^{15} to 5×10^{17} cm^{-3}. Beyond 1×10^{17} cm^{-3}, the efficiency values are nearly constant, reaching a maximum of 27.96% for carrier density equal to 1×10^{17} cm^{-3}.

The J_{SC} of the cell is given as follows:

$$J_{sc}\,(mA/cm^2) = \overbrace{\left(\frac{D_n}{L_n N_a} qN_C N_V e^{-\frac{E_g}{KT}} + \frac{D_p}{L_p N_d} qN_C N_V e^{-\frac{E_g}{KT}}\right)}^{J_O}\left(e^{\frac{q\,V_{OC}}{BKT}} - 1\right) \quad (1)$$

The cell's V_{OC} (open-circuit-voltage) is represented by:

$$V_{OC}\,(mV) = \frac{BKT}{q}\ln\left(1 + J_{SC}\, e^{-\frac{E_g}{KT}}\right) \quad (2)$$

The fill factor (*FF*) of the cell is given by:

$$FF\,(\%) = \frac{J_M \times V_M}{J_{SC} \times V_{OC}} \times 100 \quad (3)$$

The η (%) of a photovoltaic device is given as:

$$\eta(\%) = \frac{P_{out}}{P_{in}} = \frac{V_{oc} J_{sc} FF}{P_{in}} \times 100 \quad (4)$$

Where, the hole/electron length of diffusion, Boltzmann constant, temperature, charge of electron, electron/hole diffusion coefficients, maximum current density, maximum voltage, minority carrier current densit, output power, diode ideality factor, and input power are denoted by L_n/L_p, K, T, q, D_n/D_p, J_M, V_M, J_o, P_{out}, B, and P_{in}.

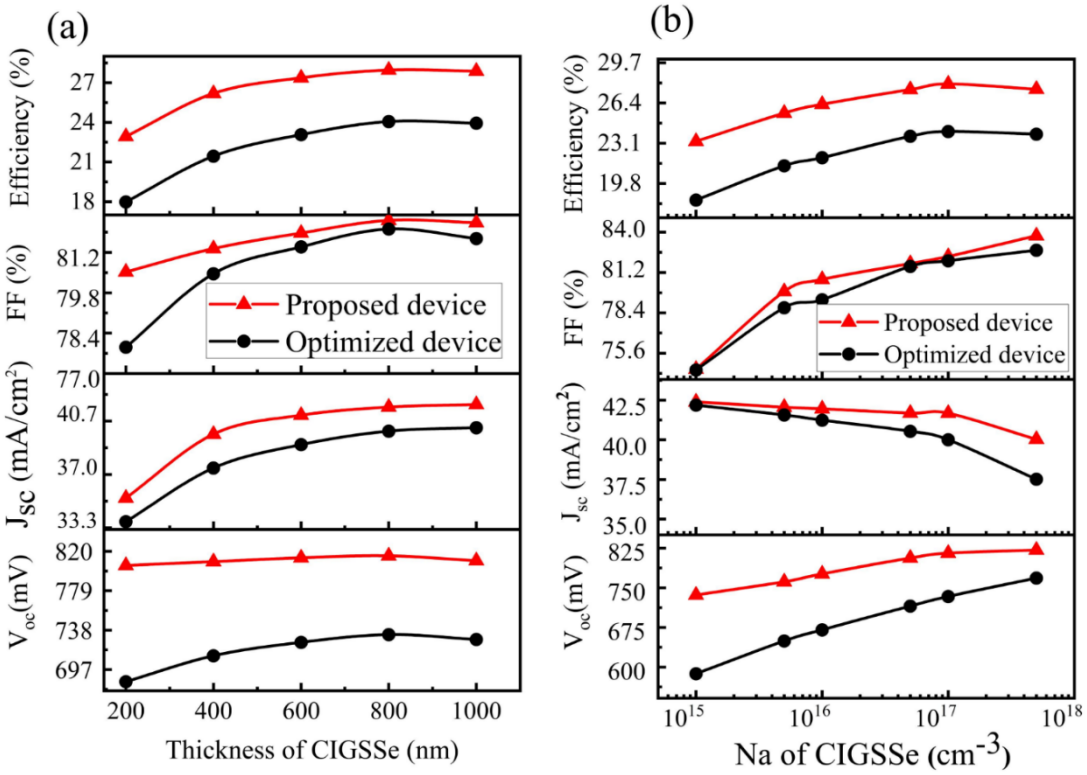

Fig. 6. Variant of V_{OC}, J_{SC}, FF and efficiency by the variation of (a) thickness and (b) donor doping density of the absorber CIGSSe layer.

4.5. Falling of *J-V* plot and EQE by the variation of CIGSSe acceptor doping density

The ratio of the absorbing photons and output charge carrier kanow as a EQE. Figures 7(a) and (b) illustrate the impact of *J-V* plot and EQE against wavelength spectra for various CIGSSe layer N_a concentrations. Eq . (5) mentioned below shows that EQE is directly correlated to the J_{SC}. So, increment in the N_a density from 1×10^{15} to 5×10^{17} cm^{-3} results in reduction in hole collections at the CIGSSe absorber layer that will increase the depletion width at the *n*-side and also increases the J_O. The CIGSSe layer-based proposed photovoltaic device reveals extreme efficiency conversion at N_a = 1×10^{17} cm^{-3}.

$$EQE(\lambda) = \frac{J_{sc}(mA/cm^2) = \overbrace{\left(\frac{D_n}{L_n N_a} A N_C N_V e^{-\frac{1.24}{KT\lambda(\mu m)}} + \frac{D_p}{L_p N_d} A N_C N_V e^{-\frac{1.24}{KT\lambda(\mu m)}}\right)}^{J_O}\left(e^{\frac{qV_{OC}}{BKT}} - 1\right)}{\varphi(\lambda)} \quad (5)$$

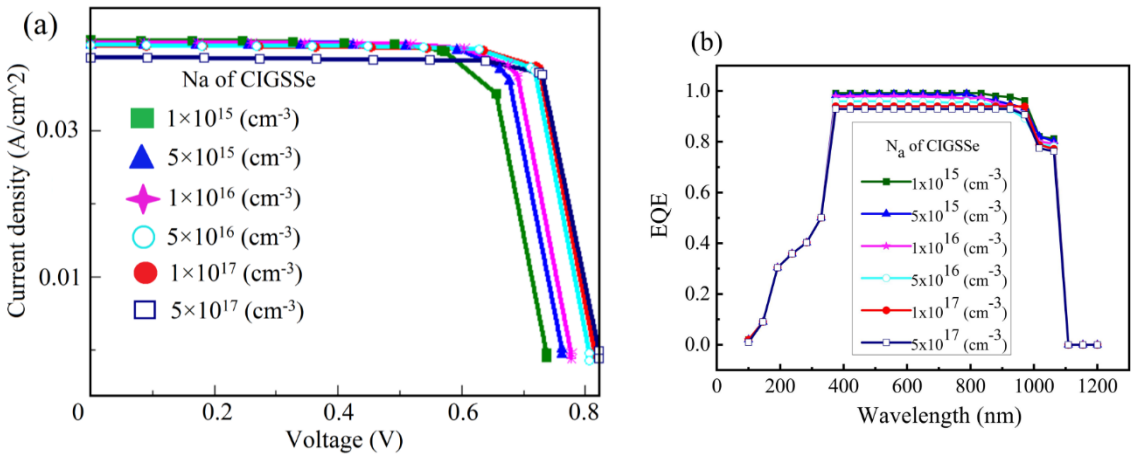

Fig. 7. Variation of (a) *J-V* plot and (b) EQE versus wavelength spectra by the variation of acceptor CIGSSe doping density of the proposed device.

4.6. Assessment of basic optimised and proposed photovoltaic devices

The photovoltaic properties of basic optimised and proposed devices are compared in Figs. 8(a)-(b) in terms of EQE against wavelength and *J-V* plot. The proposed photovoltaic parameters performance comparison with recently published research is shown in Table 4. The results indicate that the proposed photovoltaic device performs better than the recently published study.

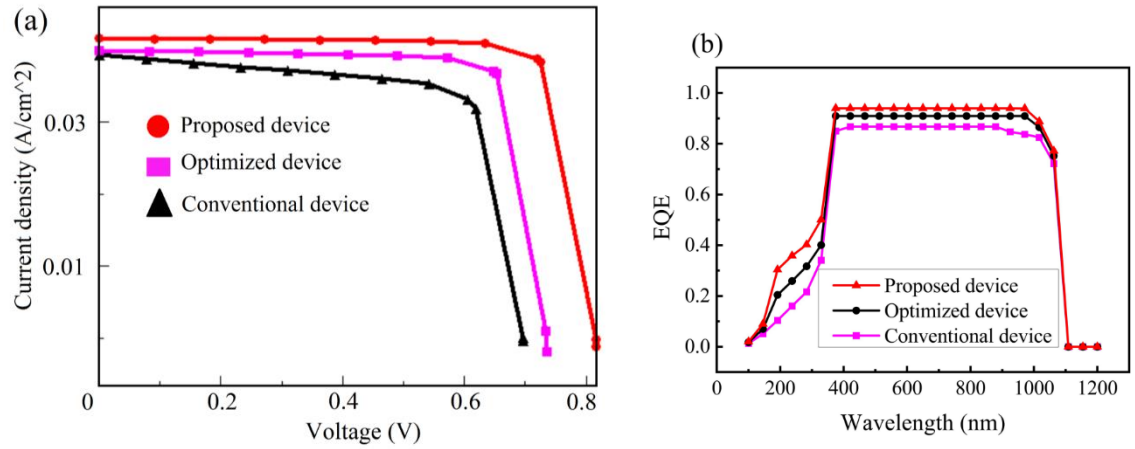

Fig. 8. (a) *J-V* plot and (b) EQE versus wavelength performance comparison of the basic, optimised and proposed photovoltaic device.

Table 4: Analysing the electrical characteristics of recently published and proposed TFSC devices.

Thickness (nm)/materials of the Front layer	Thickness(nm)/ materials of the buffer layer	Thickness(nm)/materials of the absorber layer	Thickness(nm)/ materials of BSF or HTL	V_{OC} (mV)	J_{SC} (mA/cm^2)	*FF* (%)	η (%)	Year/References
700/Al-ZnMgO	124/ZnMgO	2200/CIGSSe	NA	695.00	39.30	73.16	20.00	2018/[23]
200/Al-ZnO	100/i- ZnO 50/CdS	1000/ CIGS	NA	805.3	34.47	84.11	23.35	2022/[1]
300/ZnO:Al	50/ZnO 30/ZnMgO	800/CIGS	1200/CIGS	900	36.13	81.61	26.78	2022/[46]
150/ZnO	50/CdS	600/CIGS	10/MoS_2	783	40.30	84.97	26.81	2022/[14]
100/ZnMgO:Al	50/ZnMgO	1000/CIGSSe	50/CZTGSe	807.9	41.61	82.20	27.63	2021/[13]

50/ZnO:B	10/ZnMnO	2500/CIGSSe	10/Cu_2O	807.9	43.95	81.29	28.86	2021/[12]
100/ZnMgO:Al	20/ZnMgO	800/CIGSSe	NA	730.4	39.81	81.44	24.06	Optimised
100/ZnMgO:Al	20/ZnMgO	800/CIGSSe	100/Perovskite	815.3	41.67	82.31	27.96	Proposed

4. Conclusion

The current research examines the consequences of the perovskite HTL as a back-contact layer on the proposed photovoltaic device. At the start of the work, the photovoltaic results of the conventional photovoltaic device structures are validated by the AFORS-HET software simulation tool. Further, by optimising the thickness and doping density of the conventional photovoltaic device's Front , buffer, and absorber layers, the efficiency, V_{OC}, *FF*, and J_{SC} are enhanced. The conventional photovoltaic device has shown some drawbacks, like photogenerated leakage current due to the absence of HTL. Here, a novel structure is designed using perovskite HTL in the conventional photovoltaic device. The new structure was designed by inserting perovskite HTL material between the back ohmic contact and the CIGSSe layer. The newly proposed photovoltaic device improves photovoltaic characteristics like η=27.96%, V_{OC}=815.3 mV, *FF*=82.31, and J_{SC}=41.67 mA/cm^2 while reducing the photogenerated reverse saturation current.

REFERENCES:

1. M. Nakamura, K. Yamaguchi, Y. Kimoto, Y. Yasaki, T. Kato, H. Sugimoto, Cd-free Cu (In, Ga)(Se, S)$_2$ thin-film solar cell with record efficiency of 23.35%, IEEE Journal of Photovoltaics 9(6) (2019) 1863-1867.
2. Movla H. Optimization of the CIGS based thin film solar cells: numerical simulation and analysis. Optik 2013;124:5871e3.
3. H. Li, F. Qu, H. Luo, X. Niu, J. Chen, Y. Zhang, W. Wang, Engineering CIGS grains qualities to achieve high efficiency in ultrathin Cu (In_xGa_{1-x}) Se_2 solar cells with a single-gradient band gap profile, Results Phys. 12 (2019) 704–711.
4. Y.T. Shih, Y.C. Tsai, D.Y. Lin, Synthesis and characterisation of $CuIn_{1-x}G_xSe_2$ semiconductor nanocrystals, Nanomaterials 10 (10) (2020) 2066.
5. T. Ghorbani, M. Zahedifar, M. Moradi, E. Ghanbari, Influence of affinity, band gap and ambient temperature on the efficiency of CIGS solar cells, Optik 223 (2020), 165541.
6. B. Barman, P.K. Kalita, Influence of back surface field layer on enhancing the efficiency of CIGS solar cell, Sol. Energy 216 (2021) 329–337.
7. T. Nishimura, J. Chantana, A. Mavlonov, Y. Kawano, T. Masuda, T. Minemoto, Device design for high performance bifacial Cu(In,Ga)Se_2 solar cells under front and rear illuminations, Sol. Energy 218 (2021) 76 84.
8. P. Veluchamy, M. Tsuji, T. Nishio, T. Aramoto, H. Higuchi, S. Kumazawa, A. Hanafusa, A pyrosol process to deposit large-area SnO_2:F thin films and its use as a transparent conducting substrate for CdTe solar cells, Solar Energy Mater. Solar Cell. 67 (2001) 179–185.
9. T. Nishimura, J. Chantana, A. Mavlonov, Y. Kawano, T. Masuda, T. Minemoto, Device design for highperformance bifacial Cu(In,Ga)Se_2 solar cells under front and rear illuminations, Solar Energy 218 (2021) 76-84.
10. B. Barman, P. K. Kalita, Influence of back surface field layer on enhancing the efficiency of CIGS solar cell. Solar Energy 216 (2021) 329-337.
11. M. Nakamura, K. Yamaguchi, Y. Kimoto, Y. Yasaki, T. Kato, H. Sugimoto, Cd-free Cu (In, Ga)(Se, S)$_2$ thinfilm solar cell with record efficiency of 23.35%, IEEE Journal of Photovoltaics 9(6) (2019) 1863-186.
12. Priya, S. N. Singh, Enhancement of efficiency and external quantum efficiency of CIGSSe solar cell by replacement and inserting buffer and Cu_2O ER-HTL layer, Superlattices and Microstructures 152 (2021) 106840.
13. R. Kumar, A. Kumar, Performance Enhancement of ZnMgO:Al/ZnMgO/CIGSSe Solar Cell With the Combination of CZTGSe HT-ERL Layer, Journal of Electronic Materials 51 (2022) 84-103.
14. K. Patel, R. Mishra, S. K. Soni, Performance enhancement of CIGS solar cell with two dimensional MoS_2 hole transport layer, Micro and Nanostructures 165 (2022) 195-207.
15. R. Kumar, A. Kumar, Efficiency improvement of ZnMgO/CIGSSe heterojunction solar cell by using double graded Cu_2O ER-HTL and $CeMgO_2$ HR-ETL materials, Optical Materials 131 (2022) 112697.
16. R. Kumar, A. Kumar, K. Saurabh, Numerical optimisation of ZnMgO/ CIGS based heterojunction solar cells via change of Buffer and BSF layer" In Proceedings of the International Conference on Industrial and Manufacturing Systems (CIMS-2020) (pp. 409-419). Springer Cham.
17. Priya, A. Prakash, S. N. Singh, R. Kumar, Influence of $SnMnO_2$ Front layer on enhancing the performance of CIGSSe thin-film solar cell. Optik, (2022) 169662.

18. Priya, A. Prakash, S. N. Singh, Impact of ZnMnO buffer and $SnMnO_2$ Front layer on enhancing the performance of CIGSSe thin-film solar cell. Optical Materials, 123, (2022), 111690.
19. H. Wen, X. Luo, Tuning bandgaps of mixed halide and oxide perovskites $CsSnX_3$ (X= Cl, I), and $SrBO_3$ (B= Rh, Ti). Applied Sciences, 11(15), (2021), 6862.
20. Bag, R. Radhakrishnan, R. Nekovei, R. eyakumar, effect of absorber layer, hole transport layer thicknesses, and its doping density on the performance of perovskite solar cells by device simulation, Solar Energy 196 (2020)
177-182.
21. G. Xing, N. Mathews, S. Sun, S.S. Lim, Y.M. Lam, M. Gratzel, S. Mhaisalkar, T.C. Sum, Long-range balanced electron and hole-transport lengths in organic inorganic CH3NH3PbI3, Science 342 (2013) 344-347.
22. S. D. Stranks, G. E. Eperon, G. Grancini, C. Menelaou, M. J. P. Alcocer, T. Leijtens, L. M. Herz, A. Petrozza, H. J. Snaith, Electron hole diffusion lengths exceeding 1 micro-meter in an organometal trihalide perovskite absorber, Science 342 (2013) 341-344.
23. J. Chantana, T. Kato, H. Sugimoto, T. Minemoto, 20% efficient $Zn_{0.9}Mg_{0.1}O$:Al/$Zn_{0.8}Mg_{0.2}O$/Cu(In,Ga)$(S,Se)_2$ solar cell prepared by all-dry process through a combination of heat-light-soaking and light-soaking processes, ACS applied materials & interfaces 10(13) (2018) 11361 11368.
24. J. Chantana, T. Kato, H. Sugimoto, T. Minemoto, Aluminum-doped $Zn_{1-x}Mg_xO$ as transparent conductive oxide of Cu (In, Ga)(S, $Se)_2$-based solar cell for minimising surface carrier recombination, Progress in Photovoltaics: Research and Applications 25(12) (2017) 996-1004.
25. J. G. Lu, S. Fujita, T. Kawaharamura, H. Nishinaka, Y. Kamada, T. Ohshima, Carrier concentration induced bandgap shift in Al-doped $Zn_{1-x}Mg_xO$ thin films, Applied physics letters 89(26) (2006) 262107,.
26. M. Heinemann, C. Heiliger, Auger recombination rates in ZnMgO from first principles, Journal of Applied Physics 110(8) (2011) 083103.
27. D. Muchahary, S. Maity, High-efficiency thin film ZnMgO/ZnO solar cell simulation approach: Temperature dependency, BSF and efficient small signal analysis, Superlattices and Microstructures 109 (2017) 209-216.
28. S. Gadallah, M. M. El-Nahass, Structural, optical constants and photoluminescence of ZnO thin films grown by sol-gel spin coating, Advances in Condensed Matter Physics 2013 (2013), (Article ID 234546, 11 pages).
29. K. Ellmer, Resistivity of polycrystalline zinc oxide films: current status and physical limit, Journal of Physics D: Applied Physics 34(21) (2001) 3097.
30. N. Najafi, S. M. Rozati, Resistivity reduction of nanostructured undoped zinc oxide thin films for Ag/ZnO bilayers using APCVD and sputtering techniques, Materials Research 21(3) (2018) 1-10.
31. J. Pettersson, C. Platzer-Bjorkman, U. Zimmermann, M. Edoff, Baseline model of graded-absorber Cu(In,Ga)Se_2 solar cells applied to cells with $Zn_{1-x}Mg_xO$ buffer layers, Thin Solid Films 519(21) (2011) 7476-7480.
32. Z. J. Othman, A. Matoussi, Morphological and optical studies of zinc oxide doped MgO, Journal of Alloys and Compounds 671 (2016) 366-371.
33. Berenguier, N. Barreau, A. Jaffre, D. Ory, J. F. Guillemoles, J. P. Kleider, L. Lombez, Defects characterisation in thin films photovoltaics materials by correlated high-frequency modulated and time resolved photoluminescence: An application to Cu(In,Ga)Se_2, Thin Solid Films 669 (2019) 520-524.
34. G. X. Liang, P. Fan, P. J. Cao, Z. H. Zheng, D. P. Zhang, Properties of $CuInGaSe_2$ thin-film prepared from multiple layers via ion beam sputtering method, ECS Solid State Letters 3(3) (2013) 23-26.
35. J. Liu, D. M. Zhuang, M. J. Cao, C. Y. Wang, M. Xie, X. L. Li, Preparation and characterisation of Cu (In, Ga) Se_2 thin films by selenization of $Cu_{0.8}Ga_{0.2}$ and In_2Se_3 precursor films, International Journal of Photoenergy 2012 (Article ID 149210, 7 pages).
36. M. Troviano, K. Taretto, Urbach energy in CIGS extracted from quantum efficiency analysis of high performance CIGS solar cells, European photovoltaic solar energy conference (2009) 2933-2937.
37. P. Jha, A. K. Ganguli, New perovskite-related oxides having high dielectric constant: $Ln_2Ba_2CaZn_2Ti_3O_{14}$ (Ln= La and Pr), Journal of Chemical Sciences 115(5) (2003) 431-438.
38. Y. Zhou, G. Long, Low density of conduction and valence band states contribute to the high open-circuit voltage in perovskite solar cells, The Journal of Physical Chemistry C 121(3) (2017) 1455-1462.
39. F. Funabiki, Y. Toda, H. Hosono, Optical and electrical properties of perovskite variant $(CH_3NH_3)_2SnI_6$, The Journal of Physical Chemistry C 122(20) (2018) 10749-10754.
40. T. Bendib, H. Bencherif, M. A. Abdi, F. Meddour, L. Dehimi, M. Chahdi, Combined optical-electrical modeling of perovskite solar cell with an optimised design, Optical Materials 109 (2020) 110259.
41. J. Chantana, Y. Kawano, T. Nishimura, A. Mavlonov, Q. Shen, K. Yoshino, T. Minemoto, Impact of Auger recombination on performance limitation of perovskite solar cell, Solar Energy 217 (2021) 342-353.

42. J. M. Richter, M. Abdi-Jalebi, A. Sadhanala, M. Tabachnyk, J. P. Rivett, L. M. Pazos-Outon, R. H. Friend, Enhancing photoluminescence yields in lead halide perovskites by photon recycling and light out-coupling, Nature communications 7(1) (2016) 1-8.
43. Pathak, S. K. Pandey, Design, performance, and defect density analysis of efficient eco-friendly perovskite solar cell, IEEE Transactions on Electron Devices 67(7) (2020) 2837-2843.
44. T. J. Mebelson, K. Elampari, Numerical simulation for optimal thickness combination of CdS/ZnS dual buffer layer CuInGaSe2 solar cell using SCAPS 1D. Indian Journal of Science and Technology, 12(45), (2019) 1-6.
45. S. Dabbabi, T. B. Nasr, N. Kamoun-Turki, Parameters optimisation of CIGS solar cell using 2D physical modeling. Results in physics, 7, (2017) 4020-4024.
46. R. Prasad, R. Pal, U. P. Singh, Performance optimisation of single graded CIGS absorber and buffer layers for high efficiency: A numerical approach, Superlattices and Microstructures 161 (2022) 107094.